AIMS Materials Science, 8(2): 247–260.
DOI: 10.3934/matersci.2021016
Received: 21 November 2020
Accepted: 17 March 2021
Published: 01 April 2021

http://www.aimspress.com/journal/Materials

Survey

A survey on pristine and intercalation doped graphene nanoribbon interconnect for future VLSI circuits

Subhajit Das[1], Sandip Bhattacharya[2], Debaprasad Das[3,*], and Hafizur Rahaman[4]

[1] School of VLSI Technology, Indian Institute of Engineering Science and Technology, Shibpur, Howrah, West Bengal, India
[2] Dept. of Electronics and Communication Engineering, SR University, Warangal, India
[3] Dept. of Electronics and Communication Engineering, Assam University, Silchar, India
[4] School of VLSI Technology, Indian Institute of Engineering Science and Technology, Shibpur, Howrah, West Bengal, India

* **Correspondence:** Email: dasdebaprasad@yahoo.co.in.

Abstract: The paper presents a review of recent works on pristine and intercalation doped graphene nanoribbon interconnects. Since the last decade, there have been tremendous research interests on graphene-based nanoelectronics. Graphene nanoribbon (GNR) has been projected as an interconnect material to replace the traditional copper interconnects. Since graphene is a planar material, CMOS compatible processes for patterning and making contacts to it, can be developed. Though, fabricating side-contacts in multilayered GNR (MLGNR) is a challenging task, fabrication of top-contact MLGNR is technologically viable. In addition, intercalation doping in top-contact MLGNR improves effective conductivity further. A number of models have been developed to optimize emerging on-chip interconnect technologies and benchmark them against conventional technologies. In this review, physical and electrical models of pristine and intercalation doped MLGNRs have been discussed in brief. A chronological survey towards analytical and spice compatible modeling of pristine and intercalation doped top-contact (TC) and side-contact (SC) MLGNR interconnect, has been presented in this article. A brief review of experimental work on pristine and intercalated GNRs as on-chip interconnect has also been incorporated in this survey. The stability, signal integrity (SI), and power integrity (PI) analysis of pristine and intercalation doped MLGNR interconnect with the presented models have been depicted further. The performance assessments have been compared with conventional copper, and CNT-based interconnects as well. It has been concluded that the side-contact and intercalation doped top-contact MLGNRs can outperform conventional copper-based interconnects.

Keywords: interconnect; VLSI; graphene; graphene nanoribbon (GNR); intercalation; mean free path (MFP); top-contact; side-contact; fabrication; analytical modelling; circuit modeling

1. Introduction

Graphene nanoribbon (GNR) is a narrow strip of the patterned graphene sheet that has gained considerable research interest for its distinct electrical, thermal, structural, magnetic, and mechanical properties [1–11]. The properties like, linear *E-k* relationship, long mean free path (MFP), superior mobility, ideally negative temperature coefficient of resistance, and a width-dependent transport gap have made GNR a stronger alternative to the conventional copper for nano-interconnect applications [12–13]. Although GNR has very high carrier mobility [14], it is limited by different scattering mechanisms. Depending on the geometry, GNRs exhibit metallic or semiconducting property [15,16]. The transverse width of GNRs should be substantially smaller than that of the longitudinal length [17,18]. Depending upon the position of Carbon atoms at the edges, GNRs are classified as armchair and zigzag nanoribbons as depicted in Figure 1a,b. The difference in orientation at these edges of GNRs is 30° [18–20]. Subsequently, no contribution from GNR has been observed to energy states near the Fermi level of Carbon atoms as hydrogen atoms passivize the edge of the GNRs [19,20]. *N* is illustrated in Figure 1 as the number of dimers for armchair GNR as well as zigzag lines in ZZ-GNRs [12]. The width, *w* of the GNR has a direct relationship with the integer *N*, which is represented in Figure 1a, where it has been presented that, width and length of the unit cell of armchair GNRs are $w = (N + 1)\, a/2w$ and $a_T = \sqrt{3}a$. However, in the case of ZZ-GNR, these are, w and a, *w* and *a* ($w = a\sqrt{3} + \sqrt{3\ N_a/2}$) respectively, which has been shown in Figure 1b. The value of *N* is $(3p + 2)$ when an armchair GNR possesses the metallic property, and it is 3p or $(3p + 1)$, the nature is semiconducting [21]. It should be noted that p has been assumed to be an integer at this point (p = 1, 2, 3...).

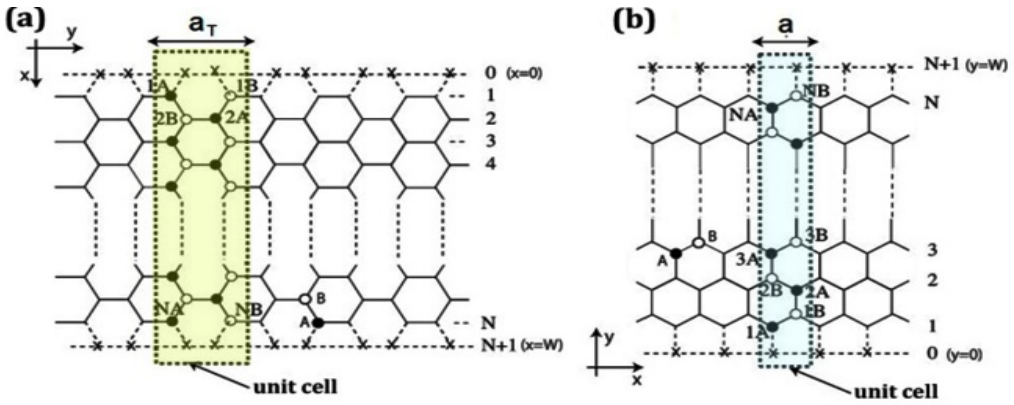

Figure 1. GNR structure with (a) armchair and (b) zigzag edges (Reprinted (adapted) from Ref. [21] with permission of American Chemical Society).

The bandgap shrinks with the increase of the width of the semiconducting GNR, and the metallic GNR has a large value of *N* [12]. The ZZ-GNR's Brillouin zone has partially flat bands due to their edge states and consequently shows zero bandgap with metallic behavior [19,20,22]. Furthermore, it is build up with three kinds of arrangements of carbon atoms; consequently, a significant difference in heat transfer capability is observed [23]. Therefore, the ZZ-metallic GNRs have attracted wide attention among researchers in the field of on-chip interconnect design [12,19,24].

The intercalation is a process of implanting molecules or ions between the large van der Waals gap of GNR layers. It has been reported in the literature that intercalation doping in bulk material shows a significant distinction from the layered materials like GNR [25,26]. Subsequently, intercalation doping in layered material upshots significant improvement in the device and interconnect-based applications [27–31]. Intercalation doping has been proved as a very powerful way to tune the attributes of MLGNRs for few reasons like, (a) the associated changes of the material properties are irreversible, (b) through this process, highest possible doping can be achieved, and (c) the amount of intercalation is controllable, and periodically run-time control has been achieved through electrochemical voltage.

With the intercalation doping, both the in-plane and interlayer (c-axis) resistances of MLGNR have been improved. Major improvement in Fermi energy, mobility, and mean free path has been achieved through Arsenic Pentafluoride (AsF_5-), Lithium (Li-), Ferric Chloride ($FeCl_3$), and Molybdenum Pentachloride ($MoCl_5$) intercalation doping. Lithium (Li-) intercalated ultrathin graphite structure is fabricated, and improvement in Fermi level and in-plane conductivity has been experimentally observed [30]. The reported values of inter-layer conductivity (σ_c) of pristine and intercalation doped graphene are presented in the literature [25,26,28,29,32] as displayed in Table 1.

Table 1. Properties of pristine and intercalation doped MLGNRs [14–15,32].

Properties	Pristine (undoped)	$FeCl_3$-intercalated	AsF_5-intercalated	Li-intercalated	$MoCl_5$-intercalated
E_f (eV)	0.2	0.6	0.68	1.5	3.4
δ_m (nm)	0.34	0.575	0.394	0.37	0.96
C-axis conductivity $(\Omega \cdot cm)^{-1}$	0.033	0.24	1.0	1.8×10^4	0.33

The rest of the article is organized as follows. Section works on modelling and analysis of GNR based interconnects presents a detailed review on modeling and analysis of GNR based interconnects. The practical works on GNR are presented in section practical works on GNR, followed by section conclusions.

2. Works on modelling and analysis of GNR based interconnects

A number of research articles have been published which demonstrate the performance of GNR interconnect in nano-scale high-speed CMOS-based design. Naeemi and Meindl [33] proposed a physics-based conductance model for graphene nanoribbon (GNR) interconnect for the first time. They also proposed a charge transport model of zigzag and armchair graphene nanoribbons [34]. Murali et al. have proposed a temperature-aware resistivity model of graphene nanoribbon interconnect [35]. Further, Naeemi and Meindl [36] have proposed a complete compact physics-based circuit model for GNR interconnect with an accurate calculation of the number of conduction

channels (N_{ch}) in a single layer GNR (SLGNR) using the close form approximation method. The equivalent single-conductor (ESC) model of MLGNR interconnect is illustrated in Figure 2 [13].

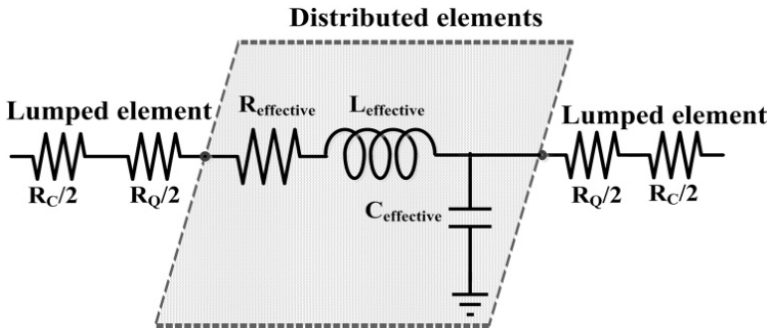

Figure 2. Basic equivalent single-conductor (ESC) model of MLGNR interconnect (Reprinted from Ref. [13] with permission of IEEE).

Nasiri et al. proposed a compact formula to calculate temperature aware number of conduction channels of graphene nanoribbons with different Fermi energy [37]. However, this approach limits the computation for a given temperature and Fermi energy only. Figure 3 shows the design route of the MLGNR as an on-chip interconnect.

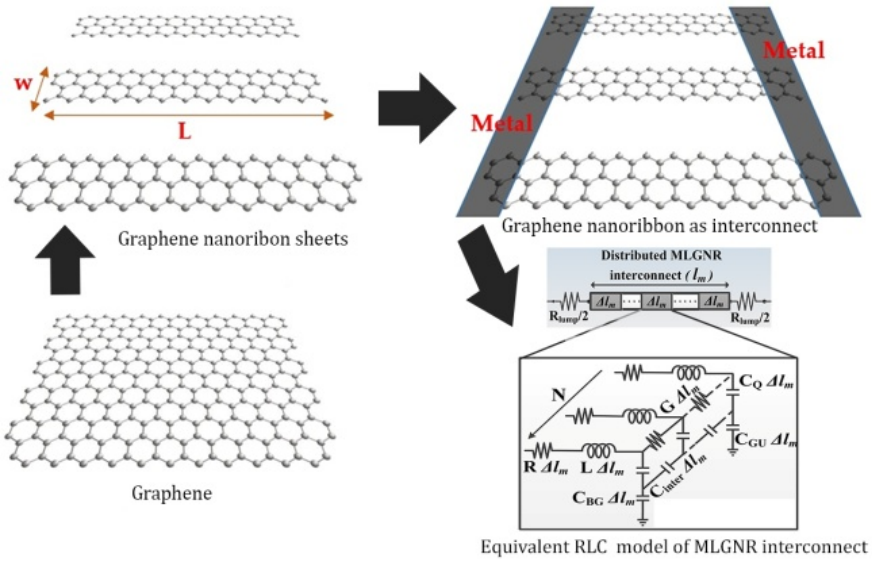

Figure 3. Schematic representation of graphene to MLGNR modeling approach.

In [28], Banerjee et al. have proposed the conductance model of GNR with tight-binding approximation and obtained a linear *E-k* relationship using Landauer formalism. Here, the delay analysis in GNR interconnects has been presented as well as the performance comparison with other interconnect materials, such as copper (Cu), tungsten (W), and CNT, has been performed. Nasiri et al. have presented stability analysis in GNR interconnects [38]. The relative stability of multilayer GNR (MLGNR) interconnects is analyzed using the Nyquist stability criterion. Their analysis shows that

by increasing the length and width, MLGNR interconnects become more stable. The crosstalk stability analysis using multilayer GNR interconnects is reported in [39]. Ramesh Kumar et al. have reported the delay, and stability analysis of multilayer GNR and multi-walled CNT interconnects [40].

Kumar et al. first proposed different contact-based modeling (top-contact and side-contact) of graphene nanoribbon-based interconnect [41]. Following the route, Nisad et al. in [42] proposed a 2D resistive model for top-contact and side-contact MLGNR interconnects. It is observed that the side-contact MLGNR (SC-MLGNR) performs better than top-contact MLGNR (TC-MLGNR) in terms of delay, power-delay product (PDP), energy-delay product (EDP), etc. reported in [40–43]. But from the fabrication point of view, the TC-MLGNR is much better than SC-MLGNR reported in [41,42]. Subsequently, to improve the performance of TC-MLGNR, intercalation becomes important. The conductance modeling of intercalation doped TC-MLGNR has been presented in [22]. Intercalation doping with Arsenic pentafluoride (AsF_5) in MLGNRs has been carried out by Xu et al., and substantial improvement in Fermi level consequently MFP and been observed [44].

A self-heating model has been proposed by Jiang et al. [45] on Lithium (Li-) and Ferric chloride ($FeCl_3$-) intercalation doped ultra-thin graphite arrangement has been fabricated as TC- interconnect and the improvement in Fermi level, and the in-plane conductivity has been experimentally observed. Das et al. proposed an electro-thermal RF model [46,47] for intercalation doped TC- as well as SC-MLGNR considering the integrated effect of distributed interconnect system based on the thermophysical property of multilayer GNR studied in the literature [48–51]. They have demonstrated superior RF performance of intercalation doped TC-MLGNR interconnect as compared to its pristine counterpart for different chip operating temperatures. Rakheja et al. [52] have compared the energy dissipation, and overall performance of graphene spin interconnects in a non-local spin-torque (NLST) circuit against the conventional CMOS-based circuit. They also reported the prospects of graphene-based interconnect that could be the replacement of copper in future microchips. The spin injection probability of electron in graphene wires has been further explored by them in [53]. The improvement of carrier transport with the help of the selective hydrogenation mechanism of edges for sub-30 nm graphene nanoribbons (GNRs) has been reported [54]. After improvement of the edges roughness, the GNRs exhibit improved transport properties. The carrier mobility has been improved up to 50% when the carrier density is cm^{-2} at room temperature.

Pan et al. [55] reported the advantage of GNR interconnect over the traditional Cu-based nano-interconnect for next-generation VLSI interconnect. They have designed a 32-bit adder using MLGNR interconnect and observed a 70% improvement in EDP. They have also demonstrated the design of the ARM processor using MLGNR interconnect and achieved 22% and 15% improvement in EDP and clock frequency, respectively. It should be noted that the benefits observed in ARM processors are highly dependent on the quality, such as the MFP and the edge roughness of the GNR.

The simultaneous switching noise (SSN) and IR-drop analysis for graphene nanoribbon-based power distribution network reported by Das et al. [56]. This paper reports the peak SSN in Cu-based interconnects 41–23% larger than that in GNR. Consequently, the peak IR-drop in GNR is 38–34% lesser than that of traditional copper wires. The propagation delay is highly affected due to SSN and IR-drop. GNR shows up to 64.49% lesser impact in the SSN generated delay in comparison with the Cu-based power networks. The reduced thickness model of MLGNR interconnect has been proposed by Bhattacharya et al. [57]. It has been demonstrated that keeping the width constant, reduced thickness of MLGNR has a lesser impact on crosstalk delay and overshoot/undershoot. The IR-drop

induced temperature aware delay fault model of CNT and GNR based power distribution networks is proposed by Das et al. and Bhattacharya et al. [58,59]. It has been observed in these works that the delay faults can be reduced using CNT as well as GNR based power interconnects at longer lengths as compared to the conventional Cu-based power interconnects. The crosstalk and gate oxide reliability analysis in GNR interconnects have been investigated by Sahoo et al. [60] and Das et al. [61]. It has been observed that electric field acceleration rises significantly at a higher temperature. This set a substantial impact on gate oxide reliability on MLGNR driven interconnect system. This thermal impact of gate oxide reliability has been reported by Das et al. [62].

The contact resistance-related issues in GNR based interconnect is very crucial in sub-nanometer technology. It may be top-contact or side-contact. The top-contact resistance for multi-layered GNR interconnect is ~4.3 kΩ reported in [41]. Leong et al. [63] reported the graphene-based devices with nickel-etched-graphene contacts, which shows considerably low contact resistance.

Signal transmission and integrity analysis on GNR based interconnect reported by Zhao et al. [64]. Signal integrity analysis of single and multi-layered GNR interconnects has been performed based on their circuit equivalent models, with crosstalk effects characterized theoretically. It has been concluded in their work that longer SLGNR interconnect with larger width results in higher crosstalk noise than that of MLGNR or Cu-based interconnects. Cui et al. [65] have analyzed signal transmission characteristics in multilayer GNR (MLGNR) interconnects for 22 nm and 14 nm technology nodes. An ESC model has been derived, and transient response is studied in their work. Another signal transmission analysis along GNR interconnects has been reported by Xu et al. [66]. Sarkar et al. have reported the UHF behavior of GNR based interconnects. They have proposed a numerical model of GNR as an on-chip interconnect to calculate the surface impedance with anomalous skin effect in high-frequency using linear dispersion relation of graphene [67,68]. Chen and Fratini et al. [69–70] have reported the distress of low-bias resistivity due to phonon-based scattering (e.g., acoustic phonon scattering (AP) and remote interfacial phonon (RIP)) with temperature. These works imprinted a significant impact on temperature-dependent models and circuit analysis of GNR as an on-chip interconnect [37,45,47,59,62].

3. Practical works on GNR

The world's first graphene-based integrated circuit (IC) was developed by IBM in the year of 2011. An article on graphene-based IC design by the IBM research group is reported by Lin et al. [3]. T. J. Watson Research Center (Microelectronics Research Laboratory) and AMO Nanoelectronics group had demonstrated the possibility of creating the graphene-based transistor [71]; this evolutionary research took the technology a step further by binding the transistor and other electronics on a single chip to build a full-fledged integrated circuit. In this work, the wafer-scaled graphene-based circuit has been reported, where graphene channel-based FET, interconnect, and inductor, were monolithically integrated on a single SiC wafer. The IC was operated as a broadband RF-mixer operative up to 10 GHz frequency range. The graphene-based system exhibited outstanding thermal stability between 300 and 400 K chip operating temperature. This integration gives an inference to a platform created by Meyer et al. in 2007 with suspended graphene [72]. The pioneering work done by IBM [3] created a perpetual impact on future research on graphene-based technology for integrated circuit applications.

Heinz and co-workers modeled as well as fabricated the monolayer graphene resonator on SiO_2 substrate to demonstrate that graphene can transduce the motion of profound resonant circuit with minimal damping [73], the comprehensive experimental arrangement of the resonator along with schematics, circuit diagram, and SEM image are portrayed in Figure 4. This study demonstrated the superiority of graphene over CNT, evaluating the reproducible electrical properties and a larger surface area for capturing the incoming mass flux. In this work, monolayer graphene flakes have been fabricated on locating on Si/SiO_2. Subsequently, atomically precise bottom-up fabrication of GNRs on a gold substrate has been demonstrated by Fasel and his team [74], which formed GNRs. This method produces GNRs with well-controlled widths and various shapes. The controllable preparation of graphene has been pioneered by Müllen and co-workers [75,76] with bottom-up organic synthesis so that it can be produced on a large scale as an on-chip VLSI interconnect. On top of that, recently, Fischer and his team demonstrated an ingenious method in Science [77] to produce metallic GNRs based on the atomically precise bottom-up synthesis.

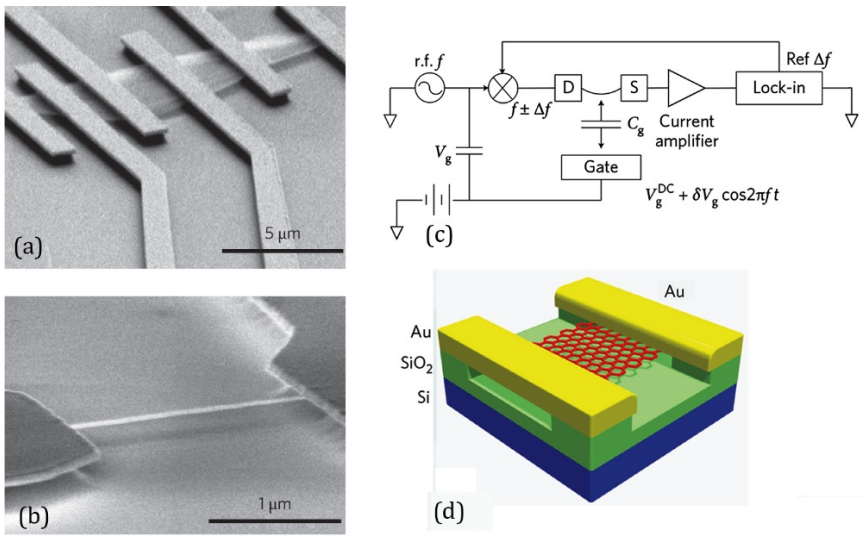

Figure 4. Experimental setup of graphene resonator on SiO_2 substrate: (a) SEM image of monolayer graphene-based resonators, (b) SEM image of suspended graphene nanoribbon, (c) Circuit diagram of graphene-based resonator where lock-in amplifier detects the current through graphene, and (d) Schematic of suspended graphene (Reprinted (adapted) from Ref. [73] with permission of Springer Nature).

Chen et al. [78] fabricated graphene-based interconnects with CMOS-based mixed-signal application, as shown in Figure 5. The graphene layers have been moved to the substrate with the help of the poly-methyl-methacrylate (PMMA) assisted method, which has been demonstrated through the progression flow chart of Figure 5a. Subsequently, graphene-based interconnects and Ti-based via have been developed with CMOS-compatible fabrication methodology. Cr/Au has been used as the contact metal of graphene-based interconnects, as shown in Figure 5b. An optical image has been captured demonstrating the graphene-based interconnects on the top layer of the ring oscillator array in CMOS based process (Figure 5c,d).

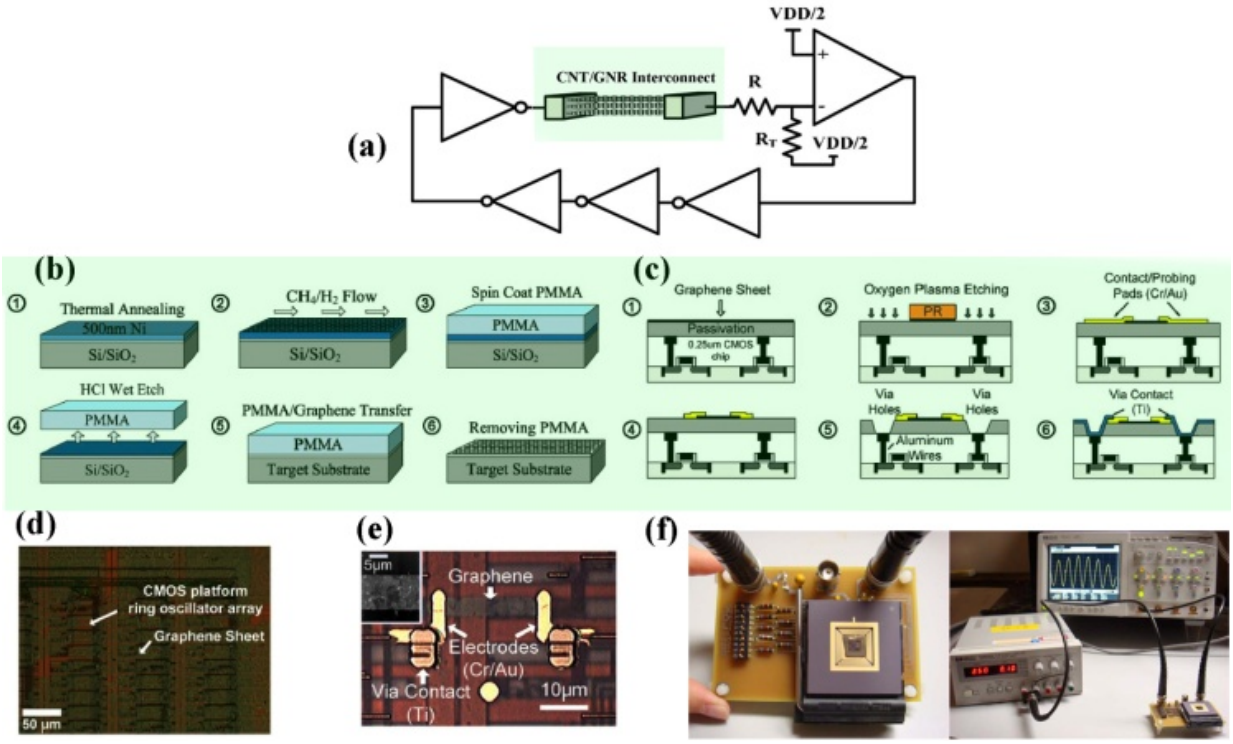

Figure 5. Process flow of on-chip graphene interconnect fabrication. (a) Ring oscillator circuit with graphene-based interconnect, (b) CVD-grown graphene transferred to substrate, (c) integration of graphene with CMOS circuitry of ring oscillator, (d) optical image of (a), (e) optical image of single graphene interconnect as a subset of (a). (Inset) AFM image of Si/SiO_2 substrate-based graphene stripes (Reprinted from Ref. [78] with permission of IEEE).

Han et al. [79] of the IBM research group reported the graphene-based on-chip RF receiver circuit, which has been integrated with a high-performance 3-stage RF amplifier, filter, and down-converter mixer module. This work revealed the use of the graphene-based system for high-end RF communication of 4.3 GHz bandwidth. Among a number of methods which have been reported to obtain intercalation doping in MLGNR, specifically chemical and electro-chemical intercalation method have been subjugated in practical implementation. Each of them is further subdivided into the categories depending upon the base of the intercalation species. As an example, when the chemical vapor transport method has been adopted for the chemical intercalation method, it is categorized as gas-phase intercalation; on the other hand, wet chemical methods are classified as liquid phase intercalation. Solid-state electrolyte intercalation and liquid electrolyte intercalation are the categories of electro-chemical intercalation doping. Intermittently molten metal (salt) intercalation doping (Li in few-layer graphene) has been reported in experimental reports [25,80], whereas Crommie et al. demonstrated intercalation of C60 into a single fold in graphene in [81]. Figure 6 provides a summary of the field of intercalation doping of 2D materials.

Recently, Jiang et al. demonstrated the CVD-grown and $FeCl_3$- intercalation-doped MLGNR for superior interconnect application [30]. MLGNR layer was first transferred to the Si- substrate. Subsequently, the Ni/Au-based alloy contacts were built for the measurement of resistivity, as shown

in the flow of Figure 7. $FeCl_3$ intercalation doping was carried out at 633 K and ~1.4 atmospheric pressure for 10 h in an Argon atmosphere, as shown in Figure 7i,j [30].

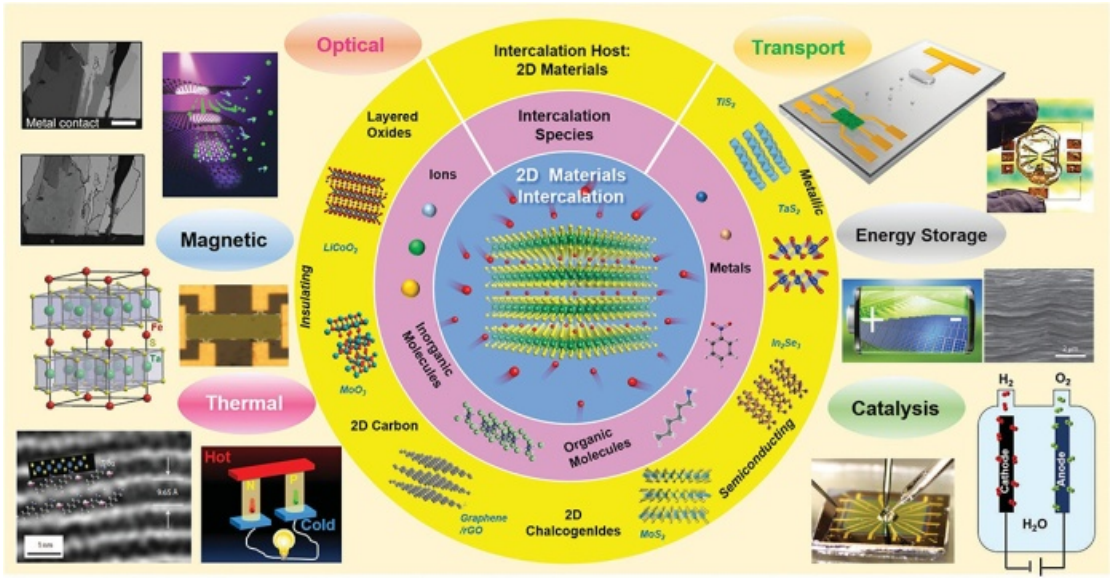

Figure 6. Summary of the intercalation of 2D materials, intercalation types, properties, and applications (Republished from Ref. [27] with permission of Royal Society of Chemistry).

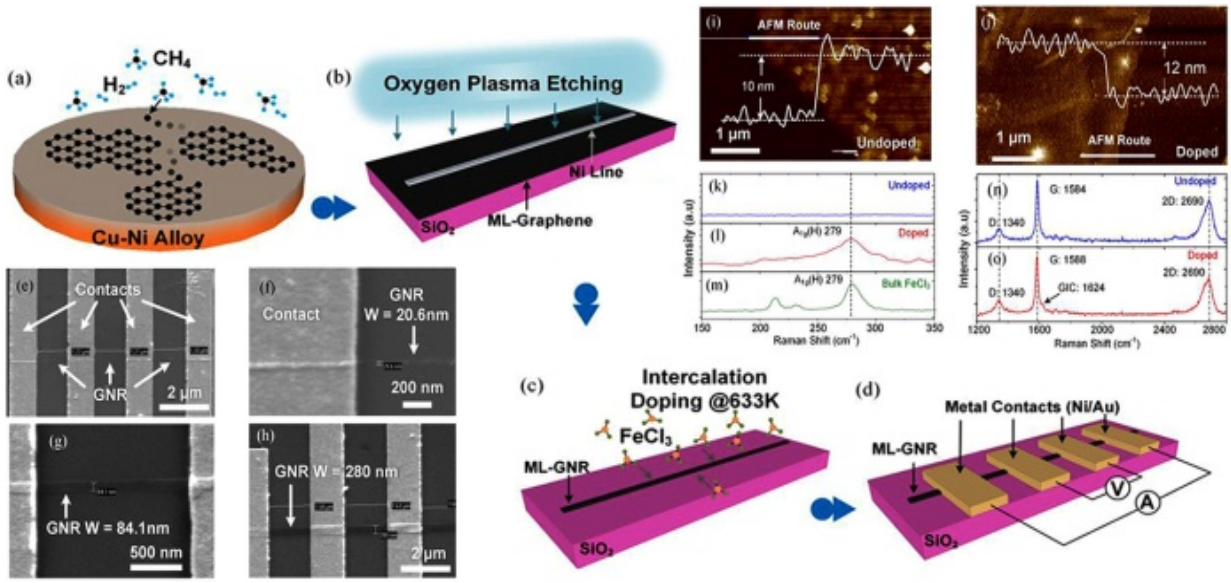

Figure 7. (a) Summery of ML-graphene fabrication, (b) ML-graphene transferred on SiO_2 substrate followed by oxygen plasma etching, (c) $FeCl_3$ intercalation at 633 K, (d) Four-probe test structures, SEM images of (e) the test structure with patterned GNR, (f–h) GNRs. AFM image of (i) pristine ML-graphene and (j) $FeCl_3$ intercalated ML-graphene shows 20% increase in thickness post-doping of 10 h; The Raman spectrum of (k,n) pristine one,(l,o) $FeCl_3$-intercalated one and (m) $FeCl_3$ (Reprinted (adapted) from Ref. [30] with permission of American Chemical Society).

4. Conclusion

A detailed literature review on graphene-based nano-interconnects is presented in this article. At first, the modeling works on GNR interconnects with different contact models are discussed. Several analysis works are reviewed thoroughly for the applicability of GNR as a nano-interconnect for future generation VLSI circuits. Next, the GNR growth technologies are presented along with different process technology. As prospective mend of nano-interconnect application, intercalation doped GNR has been emphasized and discussed with its experimental and model development outline in this review. In a nutshell, this article provides a scientific survey in favor of pristine and intercalation doped layered graphene nanoribbons as a potential candidate among nano-interconnects of future integrated circuit-based applications.

Acknowledgments

This work has been partially supported by SMDP-C2SD, DeitY, MCIT, India.

Conflict of interest

The authors declare no conflict of interest.

References

1. Novoselov KS, Geim AK, Morozov SV, et al. (2004) Electric field effect in atomically thin carbon films. *Science* 306: 666–669.
2. Mak KF, Lui CH, Heinz TF (2010) Measurement of the thermal conductance of the graphene/SiO_2 interface. *Appl Phys Lett* 97: 221904.
3. Lin Y, Garcia A, Han S, et al. (2011) Wafer-scale graphene integrated circuit. *Science* 332: 1294–1297.
4. Avouris P, Chen Z, Perebeinos V (2010) Carbon-based electronics, In: Rodgers P, *Nanoscience and Technology: A Collection of Reviews from Nature Journals*, World Scientific Publishing, 174–184.
5. Van Noorden R (2006) Moving towards a graphene world. *Nature* 442: 228–229.
6. Berger C, Song Z, Li T, et al. (2004) Ultrathin epitaxial graphite: 2D electron gas properties and a route toward graphene-based nanoelectronics. *J Phys Chem B* 108: 19912–19916.
7. Jung J, MacDonald AH (2010) Magnetoelectric coupling in zigzag graphene nanoribbons. *Phys Rev B* 81: 195408.
8. Wang Y, Cheng HP (2011) Interedge magnetic coupling in transition-metal terminated graphene nanoribbons. *Phys Rev B* 83: 113402.
9. Georgantzinos SK, Giannopoulos GI, Katsareas DE, et al. (2011) Size-dependent non-linear mechanical properties of graphene nanoribbons. *Comp Mater Sci* 50: 2057–2062.
10. Faccio R, Denis PA, Pardo H, et al. (2009) Mechanical properties of graphene nanoribbons. *J Phys-Condens Mat* 21: 285304.
11. Slota M, Keerthi A, Myers WK, et al. (2018) Magnetic edge states and coherent manipulation of graphene nanoribbons. *Nature* 557: 691–695.

12. Wakabayashi K, Dutta S (2012) Nanoscale and edge effect on electronic properties of grapheme. *Solid State Commun* 152: 1420–1430.
13. Naeemi A, Meindl JD (2007) Conductance modeling for graphene nanoribbon (GNR) interconnects. *IEEE Electr Device L* 28: 428–431.
14. Dorf RC, Bishop RH (2005) *Modern Control Systems*, 12 Eds., Pearson.
15. Bai J, Huang Y (2010) Fabrication and electrical properties of graphene nanoribbons. *Mat Sci Eng R* 70: 341–353.
16. Xie L, Wang H, Jin C, et al. (2011) Graphene nanoribbons from unzipped carbon nanotubes: atomic structures, Raman spectroscopy, and electrical properties. *J Am Chem Soc* 133: 10394–10397.
17. Martini L, Chen Z, Mishra N, et al. (2019) Structure-dependent electrical properties of graphene nanoribbon devices with graphene electrodes. *Carbon* 146: 36–43.
18. Maffucci A, Miano G (2013) Transmission line model of graphene nanoribbon interconnects. *Nanosci Nanotech Let* 5: 1207–1216.
19. Maffucci A, Miano G (2014) Electrical properties of graphene for interconnect applications. *Appl Sci* 4: 305–317.
20. Son YW, Cohen ML, Louie SG (2006) Energy gaps in graphene nanoribbons. *Phys Rev Lett* 97: 216803.
21. de Oliveira Neto PH, Teixeira JF, da Cunha WF, et al. (2012) Electron-lattice coupling in armchair graphene nanoribbons. *J Phy Chem Lett* 3: 3039–3042.
22. Lu YF, Lo ST, Lin JC, et al. (2013) Nitrogen-doped graphene sheets grown by chemical vapor deposition: Synthesis and influence of nitrogen impurities on carrier transport. *ACS nano* 7: 6522–6532.
23. Georgantzinos SK, Giannopoulos GI, Fatsis A, et al. (2016) Analytical expressions for electrostatics of graphene structures. *Physica E* 84: 27–36.
24. Wakabayashi K, Fujita M, Ajiki H, et al. (1999) Electronic and magnetic properties of nanographite ribbons. *Phys Rev B* 59: 8271.
25. Dresselhaus MS, Dresselhaus G (2002) Intercalation compounds of graphite. *Adv Phys* 51: 1–186.
26. Enoki T, Suzuki M, Endo M (2003) *Graphite Intercalation Compounds and Applications*, Oxford University Press.
27. Wan J, Lacey SD, Dai J, et al. (2016) Tuning two-dimensional nanomaterials by intercalation: materials, properties and applications. *Chem Soc Rev* 45: 6742–6765.
28. Xu C, Li H, Banerjee K (2009) Modeling, analysis, and design of graphene nano-ribbon interconnects. *IEEE T Electron Dev* 56: 1567–1578.
29. Bao W, Wan J, Han X, et al. (2014) Approaching the limits of transparency and conductivity in graphitic materials through lithium intercalation. *Nature Commun* 5: 1–9.
30. Jiang J, Kang J, Cao W, et al. (2017) Intercalation doped multilayergraphene-nanoribbons for next-generation interconnects. *Nano Lett* 17: 1482–1488.
31. Nishad AK, Sharma R (2016) Lithium-intercalated graphene interconnects: Prospects for on-chip applications. *IEEE J Electron Dev* 4: 485–489.
32. Kinoshita H, Jeon I, Maruyama M, et al. (2017) Highly conductive and transparent large-area bilayer graphene realized by $MoCl_5$ Intercalation. *Adv Mater* 29: 1702141.

33. Naeemi A, Meindl JD (2007) Conductance modeling for graphene nanoribbon (GNR) interconnects. *IEEE Electr Device L* 28: 428–431.
34. Naeemi A, Meindl J (2008) Electron transport modeling for junctions of zigzag and armchair graphene nanoribbons. *IEEE Electr Device L* 29: 497–499.
35. Murali R, Brenner K, Yang Y, et al. (2009) Resistivity of graphene nanoribbon interconnects. *IEEE Electr Device L* 30: 611–613.
36. Naeemi A, Meindl J (2009) Compact physics-based circuit models for graphene nanoribbon interconnects. *IEEE T Electron Dev* 56: 1822–1833.
37. Nasiri S, Faez R, Moravvej-Farshi M (2012) Compact formulae for number of conduction channels in various types of graphene nanoribbons at various temperatures. *Mod Phys Lett B* 26: 1150004.
38. Nasiri S, Moravvej-Farshi M, Faez R (2010) Stability analysis in graphene nanoribbon interconnects. *IEEE Electr Device L* 31: 1458–1460.
39. Akbari L, Faez R (2013) Crosstalk stability analysis in multilayer graphene nanoribbon interconnects. *CSSP* 32: 2653–2666.
40. Kumar V, Majumder MK, Alam A, et al. (2015) Stability and delay analysis of multi-layered GNR and multi-walled CNT interconnects. *J Comput Electron* 14: 611–618.
41. Kumar V, Rakheja S, Naeemi A (2012) Performance and energy-per-bit modeling of multilayer graphene nanoribbon conductors. *IEEE T Electron Dev* 59: 2753–2761.
42. Nishad A, Sharma R (2014) Analytical time-domain models for performance optimization of multilayer GNR interconnects. *IEEE J Sel Top Quant* 20: 17–24.
43. Rai MK, Chatterjee AK, Sarkar S, et al. (2016) Performance analysis of multilayer graphene nanoribbon (MLGNR) interconnects. *J Comput Electron* 15: 358–366.
44. Xu C, Li H, Banerjee K (2009) Modeling, analysis, and design of graphene nano-ribbon interconnects. *IEEE T Electron Dev* 56: 1567–1578.
45. Jiang J, Kang J, Banerjee K (2017) Characterization of self-heating and current-carrying capacity of intercalation doped graphene-nanoribbon interconnects. *2017 IEEE International Reliability Physics Symposium (IRPS)*.
46. Das S, Bhattacharya S, Das D, et al. (2014) RF performance analysis of graphene nanoribbon interconnect, *Proceedings of the 2014 IEEE Students' Technology Symposium*, IEEE, 105–110.
47. Das S, Das D, Rahaman H (2018) Electro-thermal RF modeling and performance analysis of graphene nanoribbon interconnects. *J Comput Electron* 17: 1695-1708.
48. Shahil KM, Balandin AA (2012) Thermal properties of graphene and multilayer graphene: Applications in thermal interface materials. *Solid State Commun* 152: 1331–1340.
49. Guo Z, Zhang D, Gong XG (2009) Thermal conductivity of graphene nanoribbons. *Appl Phys Lett* 95: 163103.
50. Liao AD, Wu JZ, Wang X, et al. (2011) Thermally limited current carrying ability of graphene nanoribbons. *Phys Rev Lett* 106: 256801.
51. Georgantzinos SK, Giannopoulos GI, Anifantis NK (2016) Coupled thermomechanical behavior of graphene using the spring-based finite element approach. *J Appl Phys* 120: 014305
52. Rakheja S, Naeemi A (2012) Graphene nanoribbon spin interconnects for nonlocal spin-torque circuits: Comparison of performance and energy per bit with CMOS interconnects. I*EEE T Electron Dev* 59: 51–59.

53. Rakheja S, Kumar V, Naeemi A (2013) Evaluation of the potential performance of graphene nanoribbons as on-chip interconnects. *P IEEE* 101: 1740–1765.
54. Zheng P, Brian S, Yang Y, et al. (2013) Hydrogenation of graphene nanoribbon edges: Improvement in carrier transport. *IEEE Electron Dev L* 34: 707–709.
55. Pan C, Raghavan P, Ceyhan A, et al. (2015) Technology circuit system co optimization and benchmarking for multilayer graphene interconnects at sub-10-nm technology node. *IEEE T Electron Dev* 62: 2071–2077.
56. Das D, Rahaman H (2012) Simultaneous switching noise and IR-Drop in graphene nanoribbon power distribution networks. *2012 12th IEEE International Conference on Nanotechnology* (*IEEE-NANO*).
57. Bhattacharya S, Das D, Rahaman H (2016) Reduced thickness interconnect model using GNR to avoid crosstalk effects. *J Comput Electron* 15: 367–380.
58. Das D, Rahaman H (2012) Modeling of IR-Drop induced delay fault in CNT and GNR power distribution networks. *2012 5th International Conference on Computers and Devices for Communication* (*CODEC*), 1–4.
59. Bhattacharya S, Das S, Mukhopadhyay A (2018) Analysis of a temperature-dependent delay optimization model for GNR interconnects using a wire sizing method. *J Comput Electron* 17: 1536–1548.
60. Sahoo M, Rahaman H (2017) Analysis of crosstalk-induced effects in multilayer graphene nanoribbon interconnects. *JCSC* 26: 1750102.
61. Das S, Rahaman H (2011) Crosstalk and gate oxide reliability analysis in graphene nanoribbon interconnects. *2011 International Symposium on Electronic System Design*, 182–187.
62. Das S, Bhattacharya S, Rahaman H, et al. (2019) Modeling and analysis of electro-thermal impact of crosstalk induced gate oxide reliability in pristine and intercalation doped MLGNR interconnects. *IEEE T Device Mat Re* 19: 543–550.
63. Leong WS, Gong H, Thong JT (2014) Low-contact resistance graphene devices with nickel-etched-graphene contacts. *ACS Nano* 8: 994–1001.
64. Zhao W, Yin W (2012) Signal integrity analysis of graphene nano-ribbon (GNR) interconnects. *2012 IEEE Electrical Design of Advanced Packaging and Systems Symposium* (*EDAPS*), 227–230.
65. Cui J, Zhao W, Yin W, et al. (2012) Signal transmission analysis of multilayer graphene nano-ribbon (MLGNR) interconnects. *IEEE T Electromagn C* 54: 126–132.
66. Xu YL, Wei XC, Dai GL, et al. (2013) Analysis of signal transmission along graphene-based interconnect structures. *2013 IEEE International Wireless Symposium* (*IWS*), 1–4.
67. Sarkar D, Xu C, Li H, et al. (2011) High frequency behavior of graphene-based interconnects part i: Impedance modelling. *IEEE T Electron Dev* 58: 843–852.
68. Sarkar D, Xu C, Li H, et al. (2011) High-frequency behavior of graphene-based interconnects part ii: Impedance analysis and implications for inductor design. *IEEE T Electron Dev* 58: 853–859.
69. Chen J, Jang C, Xiao S, et al. (2008) Intrinsic and extrinsic performance limits of graphene devices on SiO_2. *Nat Nanotechol* 3: 206–209.
70. Fratini S, Guinea F (2008) Substrate-limited electron dynamics in graphene. *Phys Rev B* 77: 195415.

71. Lemme M, Echtermeyer T, Baus M, et al. (2007) A graphene field effect device. *IEEE Electr Device L* 28: 282–284.
72. Meyer JC, Geim AK, Katsnelson MI, et al. (2007) The structure of suspended graphene sheets. *Nature* 446: 60–63.
73. Chen C, Rosenblatt S, Bolotin KI, et al. (2009) Performance of monolayer graphene nanomechanical resonators with electrical readout. *Nat Nanotechnol* 4: 861–867.
74. Talirz L, Söde H, Cai J, et al. (2013) Termini of bottom-up fabricated graphene nanoribbons. *J Am Chem Soc* 135: 2060–2063.
75. Wu J, Pisula W, Müllen K (2007) Graphenes as potential material for electronics. *Chem Rev* 14: 718–747.
76. Cai J, Ruffieux P, Jaafar R, et al. (2010) Atomically precise bottom-up fabrication of graphene nanoribbons. *Nature* 466: 470–473.
77. Rizzo DJ, Veber G, Jiang J, et al. (2020) Inducing metallicity in graphene nanoribbons via zero-mode superlattices. *Science* 369: 1597–603.
78. Chen X, Akinwande D, Lee KJ, et al. (2010) Fully integrated graphene and carbon nanotube interconnects for gigahertz high-speed CMOS electronics. *IEEE T Electron Dev* 57: 3137–3143.
79. Han S, Garcia A, Oida S, et al. (2014) Graphene radio frequency receiver integrated circuit. *Nat Commun* 5: 1–6.
80. Voiry D, Yamaguchi H, Li J, et al. (2013) Enhanced catalytic activity in strained chemically exfoliated ws_2 nanosheets for hydrogen evolution. *Nat Mater* 12: 850–855.
81. Kim K, Lee Z, Malone BD, et al. (2011) Multiply folded graphene. *Phys Rev B* 83: 245433.

AIMS Press